41st Aerospace Sciences Meeting and Exhibit
6-9 January 2003, Reno, Nevada

AIAA 2003-1158

https://doi.org/10.2514/6.2003-1158

FLOW FIELD MEASUREMENT OF MIXING DRIVEN BY BUOYANCY

W.M.B. Duval*, C. Batur+, H. Zhong +
*NASA Glenn Research Center, Cleveland, Ohio 44135**
University of Akron, Dept. of Mech. Eng., Akron, Ohio 44325+

Mixing driven by buoyancy-induced flows inside a cavity consists of stretching and folding of an interface. Measurement of the flow field using particle imaging velocimetry shows that during stretching the flow field has a single elliptic point, thus dominated by a single vortex. However, global bifurcation that results in folding introduces a hyperbolic point whereby the flow field degenerates to multiple vortex interactions. The short-lived coherent structure observed during mixing which results in the Rayleigh-Taylor morphology is attributed to vortex interactions.

Introduction

The mixing characteristics of non-homogeneous fluids driven by buoyancy are important towards understanding transport phenomenon in a microgravity environment. Mixing consists of stretching and folding of an interface due to a flow field whose intensity depends on the body force. For miscible liquids, the characteristic of the flow field determines whether mass transport is governed by diffusion or bulk stirring which induces mixing. For technologically important processes, transport of mass is governed by the coupling of the body force to scalar gradients such as concentration and or temperature[1,2,3] . In order to lend insight into these classes of problems we consider a model experimental system to study mixing driven by buoyancy-induced flows. The characteristics of mixing is addressed from detail measurements of the flow field using particle imaging velocimetry (PIV), and its corresponding interface dynamics using image processing techniques.

Two-dimensional flow field measurement using PIV has become a common method[4] to quantify instantaneous velocity fields. PIV yields the Eulerian velocity field. Its advantage over alternative methods such as Stereo Imaging Velocimetry which obtains the Lagrangian history of a limited number or particles, is that it allows the measurement of complex flow patterns. The basic mono 2-D PIV system can be extended to stereo configuration to measure the 3-D flow field. Alternate methods to measure 3-D flows include stereoscopic tracking velocimetry[5]. In addition to flow field information, differential quantities can also be estimated, for example 3-D applications of PIV have been used to measure the velocity gradient tensor field for turbulent flows[6]. Measurement of complex fields occurring during fingering displacement of a miscible interface[7] has shown PIV to be a viable method for microgravity[1] experiments. The PIV technique allows detail measurement of transient flow fields which is an important application towards our model problem.

We use PIV to measure the transient characteristics of flow fields due to buoyancy- induced mixing. The Lagrangian history of the interface motion is also measured in order to corroborate the length stretch history of the interface with the flow field. For certain parametric region the intensity of the flow field causes the interface to stretch and fold. Folding of the interface generates an internal breakwave which has a whorl-like structure similar to the Rayleigh-Taylor morphology. The global bifurcation of the flow field shows that stretching is due to an elliptic point in the flow field. This event is caused by an overturning motion of the flow field. The elliptic point bifurcates to a hyperbolic point during folding which gives rise to an internal breakwave. Catastrophic annihilation of the breakwave follows due to wall collision. The collision event causes sloshing oscillation of the two fluids which decays rapidly to a stably stratified configuration. Details of the flow field show that the oscillation causes transient vortices which serve as a stirring mechanism to induce mass transport.

In the following we show the experimental set-up to measure the flow field and to quantify the interface

motion. The characteristics of mixing are deduced from corroboration of the interface dynamics and its corresponding flow field. We show that the length stretch history of the interface follows the dynamics of the flow field.

Experimental System

Mixing driven by buoyancy-induced flows is characterized by measuring two components of the system: dynamics of the flow field during stretching and folding using particle imaging velocimetry and the Lagrangian history of the interface. The experimental system used to measure the two components of the system is illustrated in Figure 1a, b. We first describe the experimental set-upused for interface tracking and then the flow field measurement.

Interface Tracking

The experimental set-up used to follow the Lagrangian history of the interface motion, measure its length, and remove the divider to establish the initial condition is shown in Figure 1a. An incoherent light source from Oriel illuminates the test cell uniformly, using a uniform light source sphere. The motion of the interface is captured by a Sony camera and recorded on a Panasonic time-lapse video recorder for off-line processing. The Stereo Image Processing Software (SIV) developed by Bethea et al. 1997[8] and the commercial CorelDraw 8 packages are used to locate the position of the interface. The steps of the algorithm to measure length of the interface are as follows: (a) a smoothing filter is implemented to remove noise from the image, (b) the trace contour filter of the package is used to detect the interface between the two fluids, and (c) the image history function is used to obtain the number of pixels of the interface. Since the length stretch of the interface is proportional to the number of pixels, its measurement is determined by counting the number of pixels. The initial condition is established from removal of the divider. The motion of the divider is controlled by specifying a desired motion trajectory on the Compumotor indexing drive that is communicated to the stepping motor. The desired motion trajectory has three parts: (i) a motion with an initial acceleration to constant velocity, (ii) a constant velocity motion, and finally (iii) a motion with a specified deceleration to a zero velocity. These steps allow precise control of the divider motion in order to establish the initial condition.

The test cell consists of an enclosure with height (H), width (L), and depth (W) with respective dimensions of 5cm, 5cm and a range of 0.2 to 5cm for the depth. The range of depth allows simulation from two-dimensions, similar to a Hele-Shaw cell, to three-dimensional configuration. For the measurement of the flow field using PIV, we used a depth (W) of 1 cm. The enclosure is made from transparent acrylic material to allow for visualization of interface dynamics. The liquids are introduced inside the two chambers through bleeding ports at the top of the cavity using a syringe with a hypodermic needle. The enclosure consists of two sections, 2.5cm each, separated by a thin polyethylene divider of thickness 0.01cm. The two compartments are sealed by keeping the test cell under compression using adjustable spring loaded clamps at the four corners of the cell, and by using a thin film of vacuum grease between the two compartments. The vacuum grease is very effective for sealing the compartments against leakage as well as to reduce friction when the divider is removed in order to establish the initial condition.

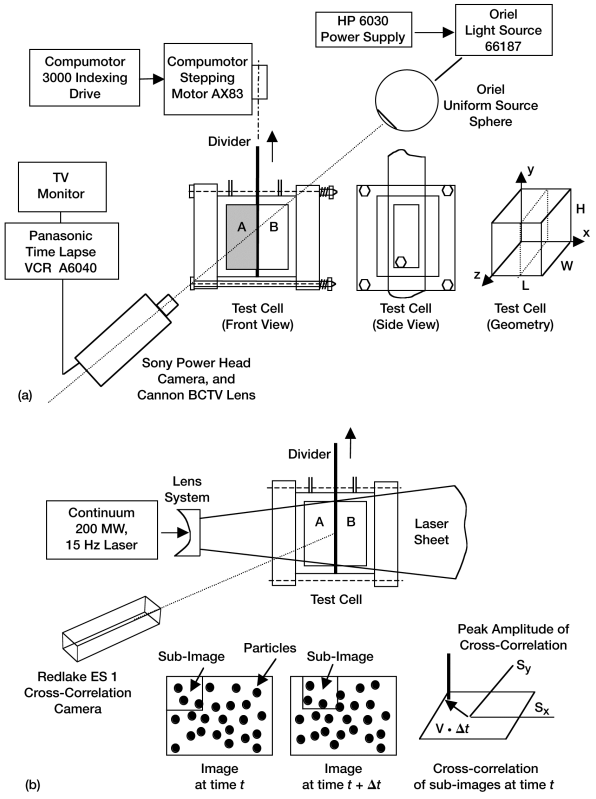

Figure 1.—(a) Experimental set-up to quantify the interface motion. (b) Experimental set-up for Particle Imaging Velocimetry.

Particle Imaging Velocimetry

Image Acquisition

Measurement of the flow field using particle imaging velocimetry (PIV) consists of image acquisition and cross correlation of the images. The sequential images

for PIV analysis are obtained by an 8-bit, (1008*1008) pixel, ES-1 cross-correlation camera made by Redlake. The camera operates at 15 Hz*;* therefore it takes two images every 133 msec. The time interval Δt between these two images can be adjusted from a few microseconds to *32 msec*. PIXCI imaging board from EPIX is used to capture the images. Timing control on the camera is established by TWAIN software package from Redlake. The test cell is illuminated by a Continuum *200 MW, 15 Hz* Nd:YAG pulsed laser. A laser sheet is generated by an optical front-end which consists of a series of plano-concave and cylindrical lenses. A typical thickness of the laser sheet in the center of the test cell is approximately one mm. An aqueous suspension of small polystyrene particles of diameter *25 μm and density 1.05 gm/cm^3*, obtained from Duke Scientific, is used to seed the flow. The seeding density is adjusted such that there will be approximately ten particles within a sub-image of (32*32) pixels.

Determination of Velocity Field

In order to determine the velocity of the seeding particles, a cross-correlation analysis is performed on two images separated by $\Delta t = 15$ *μsec*. As illustrated in Figure 1b, each image is divided into *(32*32)* pixel sub-images and a cross-correlation analysis is performed between the sub-image at time *t* and the sub-image at time t+Δt. If the intensities of sub-images are indicated by $I_1(x,y)$ and $I_2(x,y)$ then the cross correlation is determined by

$$\Gamma(s_x, s_y) = \sum\sum I_1(x,y) * I_2(x - s_x, y - s_y) \quad (1)$$

The summations are evaluated at locations *(x,y)* within sub-images; s_x and s_y denote the shifts in *x* and *y* directions, respectively. The correlation plane defined by s_x and s_y shows a peak at location (V*Δt) where V is the magnitude of the average velocity of the particles within the sub-image. The velocity field for each pair of acquired images is obtained by the PIVPROC software developed by Wernet et al. 2001[9]. Since the PIV technique determines average displacement of a group of particles in a sub-image, the resolution depends on the size of the sub-image used. A typical rule of thumb is to seed the flow field such that there are at least 10 particles within a chosen sub-region for a reliable cross-correlation analysis. In our experiments the flow field was seeded such that a sub-region of size 32×32 can be reliably used for cross correlation analysis. If the fluid needs to be low seeded one has to increase the size of the sub-image. In our experiments *(30*30)* velocity vectors are determined in *(50mm*50mm)* test cell therefore the resolution of the quantification technique is 36 velocity vectors/cm^2. The maximum particle velocity is limited by the speed of the divider, which has an upper limit of *50 cm/sec*. Since the two images are separated by $\Delta t = 15$ *μsec* then it follows that the particle with the highest velocity can travel only *750 μm*. Since the actual size of the sub-image is *1500μm* then it is expected that most of the particles will stay within the sub-image during cross-correlation.

The size of the sub-image also determines the accuracy of the velocity vectors for particles close to the boundaries. For a sub-image size of 32x32 pixels, the first velocity vector will be placed 16 pixels away from the boundaries. In our experimental set-up, 16 pixels correspond approximately to 0.8 mm distance from the test cell boundaries. One can always decrease the size of the sub-image to 16x16 pixels or even lower at the expense of a reduced number of particles within the sub-image; however, this causes a reduced resolution in the determination of velocity vectors.

One other source of experimental limitation in any PIV analysis is the lack of clear visibility of particles within a sub-region. In our experimental set-up two sources are identified for the lack of clear visibility; one is the diffraction of the laser sheet around the corners of the test cell and two is the vacuum grease that is used to avoid leakage between the two halves of the test section. In order to minimize the first problem the test cell is placed such that the minimum thickness of the laser sheet is in the middle of the test section. In addition the average thickness of the beam is adjusted to be approximately one mm. The second problem causes a lack of visibility on the vertical line separating two sides of the cell. It is estimated that the thickness of this grease seal line is approximately 0.1 mm. If the test cell is not placed orthogonal to the cameras, the image of this line can exceed 0.1 mm which further decreases the visibility.

Experimental Parameter

To investigate mixing driven by buoyancy-induced flow field, we used dilute mixtures of deuterium-oxide with de-ionized water. These two liquid pairs emulate approximately the limit of zero jump in viscosity. For color contrast we used methylene blue dye for fluid A with a concentration of 0.004% , depending on the desired contrast we either kept fluid B clear or used a red dye, bromopyrogallol red with 0.005% concentration. The specific gravity was measured for the fluid pairs using a calibrated hydrometer (Chase Instruments) with a range from 0.9950 to 1.0110 which has a precision error within ± 0.00005. The density can be calculated from the specific gravity using ($s = \rho/\rho_w$), thus ($\Delta s/\bar{s} = \Delta\rho/\bar{\rho}$) in which $\bar{s}$ and $\bar{\rho}$ are average values. The reference values for the

density of water ρ_w ($\rho_w = 0.997040\, gm/cm^3$ at 25^0C) and its kinematic viscosity[10] are taken at ambient laboratory condition. For the flow field measurement, we use $\Delta\rho/\overline{\rho} = 0.00259$ for a jump in density with a corresponding Grashof number of Gr=3.18×10^6. The dye concentration is kept the same for all fluid pairs. The contrast between the blue and clear or red region facilitated tracking of the interface as it evolves in time.

Description of Experimental Model

The experimental model for which we measure the flow field is shown in Figure 2. Two viscous miscible liquids inside an enclosure with an initially prescribed density $\rho_A > \rho_B$ is subjected to a steady body force $g_y = ng_o$. The ratio n denotes a factor by which the standard acceleration of gravity g_o on Earth (n=1) can be reduced as in an environment such as the International Space Station (n=1×10^{-6}). The density field is coupled to the body force, thus impending motion of the two fluids occurs without any stability threshold for ground-based laboratory conditions. The two fluids are separated initially by a divider. Initial contact of the two fluids is established by removing the divider with a prescribed velocity U_o. The removal of the divider introduces an impulsive disturbance on the interface for a short time duration (τ), which is much smaller than the time scale for bulk fluid motion that deforms the interface. This impulsive velocity may be described by

$$\vec{V}(L/2, y, z, t) = U_o[\delta(t) - \delta(t-\tau)] \quad (2)$$

where $\delta(t)$ represents a step function at time t=0, and $\tau = H/U_o$ is the pulse duration which depends on the prescribed pulling velocity U_o. The ideal initial condition corresponds to U_o=0.0 which means that the divider is suddenly removed without any initial disturbance. Such an ideal condition is highly desirable since it implies that symmetry would be preserved in the system as the interface deforms due to the buoyancy-induced flow field.

The total initial energy of the system,

$$E_T = \frac{1}{2}V_{ol}[\overline{\rho}U_o^2 + ng_oH\Delta\rho] \quad (3)$$

consists of the injected kinetic energy due to removal of the divider represented by the first term, and its potential energy given by the second term, in which V_{ol} =WHL and $\Delta\rho = \rho_A - \rho_B$. There is a delicate balance between the potential energy available for interface deformation and the injection kinetic energy. If the injection kinetic energy is much greater than the potential energy then the initial disturbance is superimposed on the entire time history of the transient mixing process. However, the injection kinetic energy can be tuned such that the interface evolves nearly symmetric.

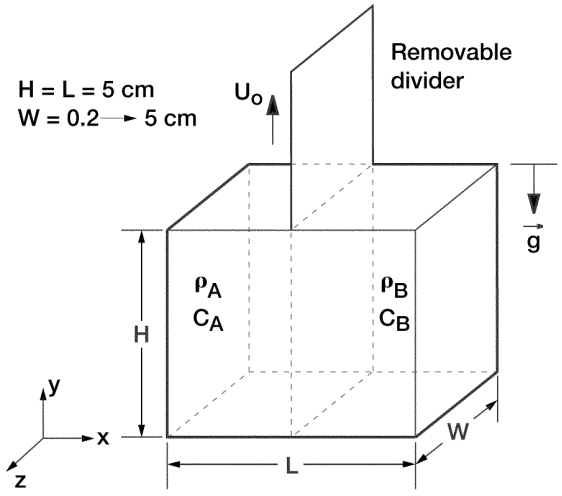

Figure 2.—Initial configuration of two fluids at an interface.

The interface motion, for the study of mixing, is described by the advection-diffusion equation

$$\frac{\partial C}{\partial t} + (\vec{V} \bullet \nabla)C = D_{AB}\nabla^2 C \quad (4)$$

This equation describes the motion of an initial line at that the interface for 2-D motion or a flat surface in 3-D. For the heavy fluid on the left C_A =1, the light fluid on the right $C_B = 0$, and the interface has the prescribed value $\overline{C} = 0.5$. The nature of the flow field determines whether or not Equation (4) is linear or nonlinear. The flow field

$$\vec{V} = \vec{V}(x, y, z, t; \Lambda) \quad (5)$$

as a function of its parametric space Λ can either be measured using PIV or computed using the approximate mean field Boussinesq equations,

$$\bar{\rho}\frac{\partial \vec{V}}{\partial t} + (\vec{V} \bullet \nabla)\vec{V} = -\nabla p + \bar{\mu}\nabla^2 \vec{V} + \rho \vec{g} \quad (6)$$

The density field in Equation (6), taken independent of pressure, is coupled to the concentration field via

$$\rho = \bar{\rho}(1 + \beta \Delta C) \quad (7)$$

in which $\beta = 1/\rho \cdot \partial\rho/\partial C$.

Since there is no change of volume during ideal mixing, the condition of incompressibility is satisfied,

$$\nabla \bullet \vec{V} = 0 \quad (8)$$

Scaling analysis shows that the parametric space becomes

$$\Lambda = \Lambda(Gr, \mathrm{Re}, Ar, Sc) \quad (9)$$

in which the Grashof number (Gr), impulsive Reynolds number (Re), aspect ratio (Ar) and Schmidt number (Sc) are defined as

$$Gr = \frac{\Delta\rho}{\bar{\rho}}\frac{n g_o H^3}{\bar{\nu}^2},\ \mathrm{Re} = \frac{U_o H}{\bar{\nu}},\ Ar = \frac{W}{H},\ Sc = \frac{\bar{\nu}}{D_{AB}} \quad (10)$$

The Grashof number, the ratio of buoyancy to viscous forces, represents the intensity of the flow field. The impulsive Reynolds number is a measure of inertial forces relative to viscous forces in the system over a short time scale relative to the advection of the interface. Note for the ideal condition[11], in which there is no initial disturbance at the interface ($U_o = 0$), the parametric space Λ_i reduces to three parameters

$$\Lambda_i = \Lambda_i(Gr, Ar, Sc) \quad (11)$$

which implies that the divider is removed instantaneously without any disturbance to the flow field.

Numerical studies[11] show that mixing can be characterized using various descriptors: length stretch ratio ($\mathcal{L}$), interface width of the mixed region and the local mixing efficiency. We use the dimensionless length stretch as a metric in our experimental studies defined as

$$\mathcal{L}(t) = \frac{\ell(t) - \ell_o}{\ell_o} \quad (12)$$

in which $\ell(t)$ is a measure of the elongation of the interface as a function of time and ℓ_o is the initial length of the interface at time zero.

Experimental Results

The mixing characteristics of two miscible liquids due to buoyancy-induced flow, from measurement of its flow field using PIV and its corresponding interface dynamics, are shown in Figure 3a-d. For $Gr = 3.18 \times 10^6$, Sc=500, Re=1500, Ar=0.2, and Sc=500, the essence of mixing is illustrated; stretching and folding of a pseudo-material interface from its initial to its final configuration. The details of interface stretching are shown in Figure 3a. According to Equation (6), the flow field is caused by a hydrostatic pressure imbalance due to the body force. Note that a body force under microgravity condition $10^{-6} g_o$ implies that the initial configuration would be stabilized as shown for t=0. The intensity of the flow field, as implied in Equation (5), gives rise to the nonlinearity in the field Equations (4,6,8), which causes stretching and folding. Insight on the effect of the impulsive velocity of the divider may be obtained from the viewpoint of a conservative system as shown in Equation (3), which says that the total initial energy consists of a balance between kinetic and potential energy. For Re=1500 the potential energy is dominant over the kinetic energy, thus as shown for $0 < t \le 3\,\mathrm{sec}$, the stretching of the interface is nearly smooth though asymmetric as the bottom fluid penetrates further than the top.

The net effect of removing the divider is shown at t=1.4 sec in Figure 3a. Two counter-rotating cells are formed near the top of the cavity superimposed on the bulk flow field caused by the buoyancy-induced flow. Within a short time interval of Δt =1.6sec, at t=3.0 sec the buoyancy-induced flow becomes dominant and the effect of the cells due to the divider motion dissipates. The rotational motion of the flow field gives birth to a vortex which has a single elliptic point at the center of the cavity. Stretching of the interface is caused primarily by the elliptic point. The computational model that considers the ideal problem also predicts that the genesis of the flow field is an elliptic point[11,12]. The fact that induced perturbations of the divider motion on the bulk flow field quickly dissipates (t=3.0 sec) show that the 2-D unsteady ideal model can adequately represent the flow field over a limited range of Reynolds number. The maximum stretching of the interface caused by overturning motion of the flow field occurs in the neighborhood of t=5 sec.

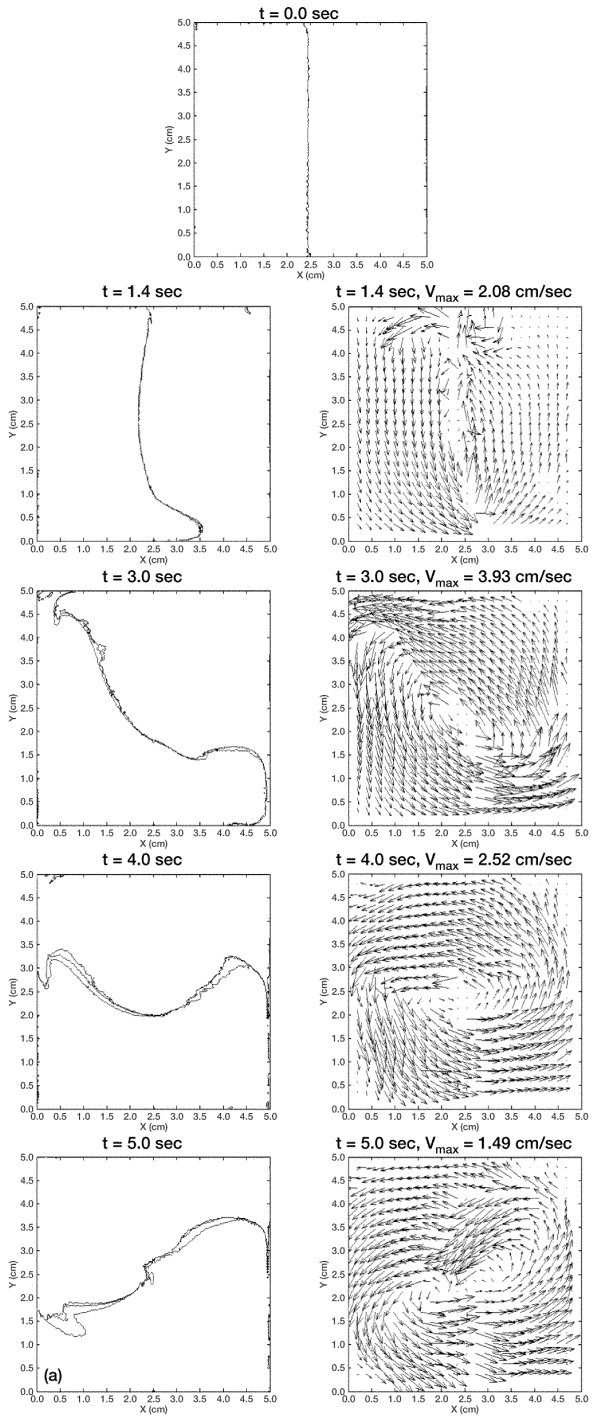

Figure 3.—(a) Stretching of interface due to buoyancy-induced flow and corresponding velocity field, $Gr = 3.18 \times 10^6$, Re = 1500, Ar = 0.2.

As the interface evolves beyond the stretching stage, folding occurs which gives rise to an internal breakwave (t=7 sec, Figure 3b), with the ubiquitous feature of the Rayleigh-Taylor morphology. The roll-up features near

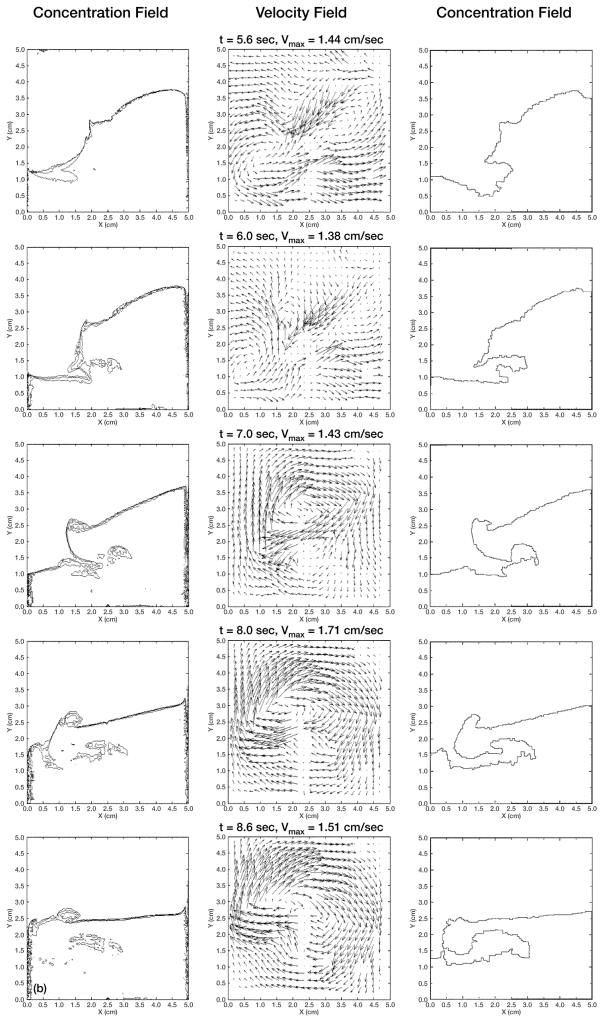

Figure 3.—(b) Folding of the interface which yields internal breakwave.

the top and bottom edge of the structure is difficult to capture using image processing. The resolution of the concentration boundary layer near the wall in another shortcoming that is difficult to assess. To show additional details, in addition to the contour levels in the left column based on intensity, we also show in the right column the missing details obtained from contour tracing. Finding two fluids with color contrast which would show a sharp image of the roll-up structure poses an experimental challenge. In addition, measurement of the length stretch of the interface is also challenging because of local mass diffusion in the neighborhood of the roll-up feature. Part of the difficulty is due to enhanced local mass transport that accompanies the folding because of the existence of hyperbolic points in the flow field. Note that at this stage asymmetry of the structure becomes more pronounced.

In contrast to the stretching event of the interface caused by a single vortex rotational motion, the folding event is caused by a global bifurcation of the flow field

which gives rise to the birth of a hyperbolic point, t=5.6 sec. The two co-rotating vortices are separated by the hyperbolic point. The vortices shown by the vector field form a homoclinic orbit. Similar homoclinic orbits have been shown[12] to occur in a similar folding structure at a lower Grashof number. The folding is caused by local stretching and contraction due to the intersection of stable and unstable manifolds near the hyperbolic point. Thus the hyperbolic point serves as an organizing center for which folding which gives rise to the short-lived coherent structure occurs.

Collision of the whorl-like structure with the wall is shown in Figure 3c. This catastrophic bifurcation annihilates the structure and produces a locally mixed or homogeneous region. The collision event (t=10.4 sec) gives rise to an explosive bifurcation which causes the birth of six vortices. This event decays through sloshing oscillations.

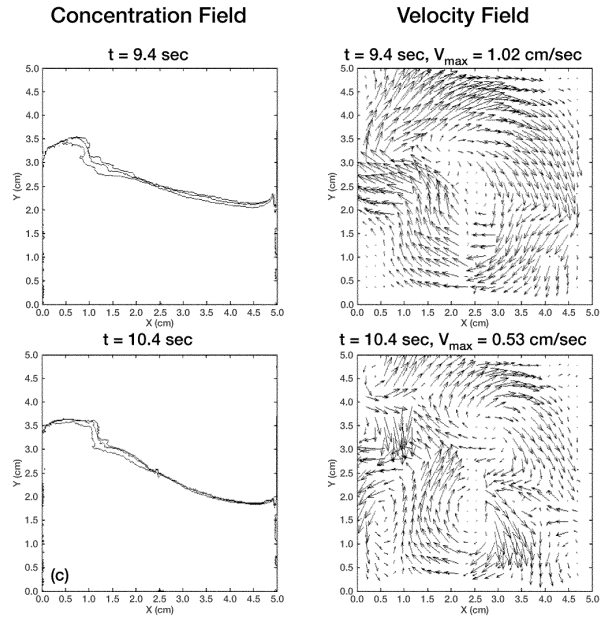

Figure 3.—(c) Catastrophic annihilation of interface break-wave due to wall collision.

In Figure 3d, we show a complete cycle of the oscillation. At the equilibrium configurations t=13.4, 17.6, 22.0 sec the flow field has a single vortex. Sloshing to the right (t= 15 sec) or the left (t=22 sec) causes destability of the flow through shearing motion which gives birth to multiple vortices. The shearing motion is caused by a global change in flow direction from a counter-clockwise (t=13.4 sec) to clockwise twist flow with each oscillation. The decay of the oscillation results in a stably stratified configuration, Figure 3e, with a locally mixed diffusive

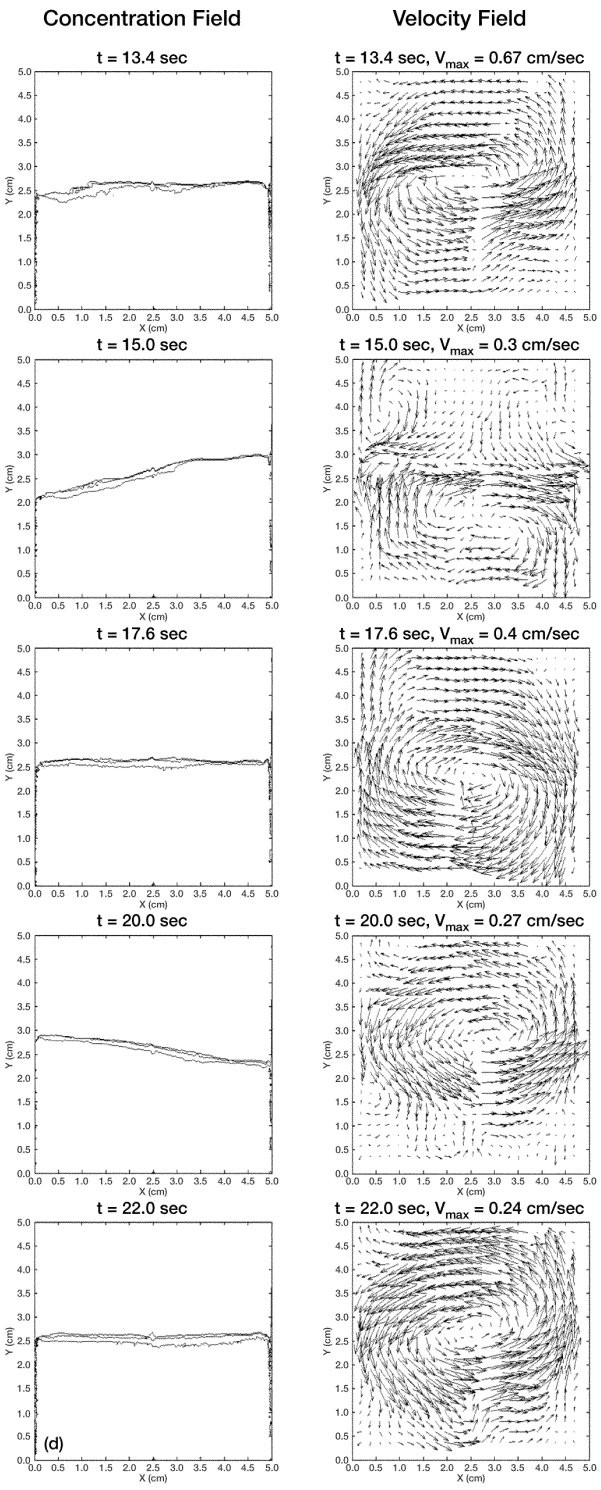

Figure 3.—(d) Oscillation of interface.

band at the interface due to local mass transport. Destabilization of the flow field due to induced shearing motion causes a slow decay of the vortices. The two fluids

then become homogeneous over a much longer diffusive time scale ($T_D = H^2/D_{AB}$).

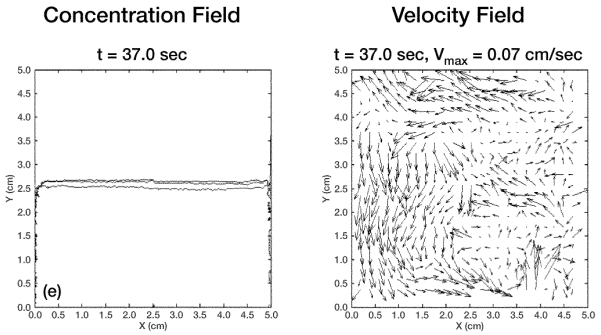

Figure 3.—(e) Stable stratification of interface.

Time history of length stretch of interface and flow field

The Lagrangian history of the length stretch of the interface contains the continuum mechanics of mixing driven by buoyancy-induced flow. The time history of length stretch $\mathcal{L}(t)$ of the interface, measured using image processing techniques, is shown in Figure 4 for Gr= 3.18×10^6 . The interface stretches exponentially over the time interval $0 < t \le 8.75\,\text{sec}$. The corresponding

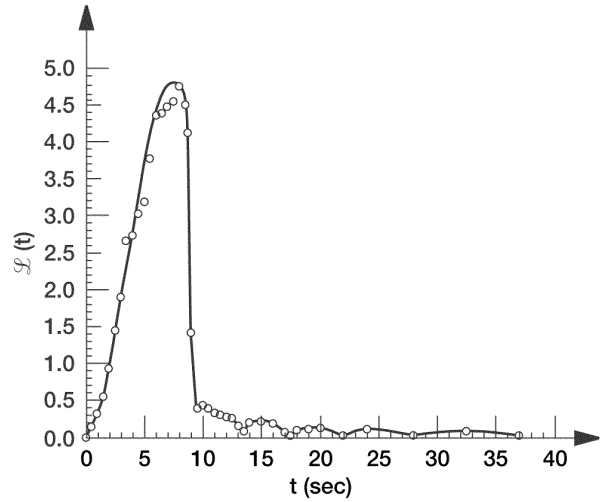

Figure 4.—Time history of length stretch of interface, Gr = 3.18×10^6, Re = 1500, Ar = 0.2.

stretching and folding events occur within the sub-intervals of $0 < t \le 5.0\,\text{sec}$ and $5.0 < t \le 8.75\,\text{sec}$ respectively. Collision of the whorl-like structure with the wall occurs over a very short time interval $8.75 < t \le 9.0\,\text{sec}$. This event causes local contraction of the interface. The time history of length stretch of the interface show a skewed-Gaussian distribution, the skewness is due to the catastrophic collision of the whorl-like structure with the wall. Due to the breakup of the interface there is a sharp drop after the maximum length stretch. The wall collision gives rise to sloshing oscillations caused by an internal traveling wave. The decay of the wave behaves similar to a damped oscillator. The decay frequency of sloshing oscillations for the interval $9.0 < t \le 40.0\,\text{sec}$ shows that the interface exhibits underdamped oscillation with a nearly periodic frequency.

The time history of the magnitude of maximum velocity, shown in Figure 5, indicates the flow field is inherently transient. The interval corresponding to stretching, folding, and collision $0 < t \le 9.0\,\text{sec}$, indicates that the flow field is aperiodic. The pulling velocity of the

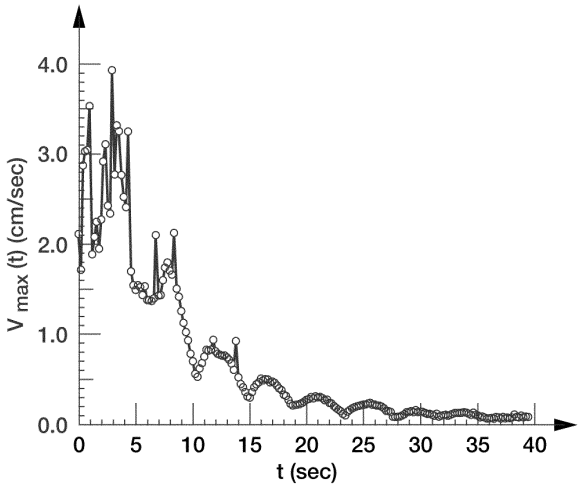

Figure 5.—Time history of maximum velocity magnitude from flow field measurement using particle imaging velocimetry, Gr = 3.18×10^6, Re = 1500, Ar = 0.2.

divider was $U_o = 3\,cm/\text{sec}$, note that the ensuing flow field has a slightly greater magnitude $V_{\max} \approx 3.3\,cm/\text{sec}$, indicating that the pulling velocity did not have much effect on the flow field. This value compares well with the prediction of a conservative system with no dissipation as in Equation (3). Equating Equation (3) to the kinetic energy of the flow field gives an expression for the maximum characteristic velocity

$$U_c = \sqrt{U_o^2 + n g_o \frac{\Delta\rho}{\bar{\rho}} H} \quad (13)$$

The predicted value $U_c = 3.6\,cm/\text{sec}$ is in agreement with measurement; the larger value is due to the neglect of

viscous dissipation. For the interval t>9 sec, as the interface approaches stable stratification, the decay frequency f=0.12Hz is in agreement with the frequency shown in Figure 4 obtained from interface motion. This implies that the motion of the flow field drives the dynamics of the interface.

Summary and Conclusions

We studied the mixing characteristics of two miscible viscous fluids driven by buoyancy-induced flows by following the Lagrangian history of the interface to measure its length stretch as well as its associated flow field using particle imaging velocimetry. The use of the PIV technique facilitated probing of the global bifurcation of the flow field We show that mixing occurs through stretching and folding of an interface when the initial potential energy that can be quantified by a Grashof number is near a critical threshold. The approach to symmetry of the short-lived coherent structure is dependent on the injected kinetic energy in the system. The attributes of the whorl-like structure can be described as an internal breakwave with a Rayleigh-Taylor morphology. Catastrophic bifurcation of the whorl-like structure occurs through wall collision. The collision event decays through sloshing oscillations with a resulting diffusive band at the interface denoting local mass transport.

The global bifurcation of the flow field shows that the genesis of stretching occurs through an elliptic point which loses stability to a hyperbolic point. The hyperbolic point serves as an organizing center for folding. The system gains stability, after the decay of sloshing oscillations. Destabilization of the flow field during sloshing through shearing motion gives birth to multiple vortices which serve as a stirring mechanism to enhance local mass transport at the interface region.

Acknowledgements

We acknowledge Code UG of NASA for support under Grant No. NAG3-2443. We thank M. Wernet and W.T. John for assistance in making the flow field measurements using particle imaging velocimetry. We also thank M. Bethea for discussions and assistance on the use of SIV software for interface tracking and L. Gumennik for instrumentation.

References

1) Gerbi, D.J., Egber, W.C., Ender, D.A., Leung, P.C.W., Rochford, K.B., Virde, J.W., Cook, E.L., "Growth of Organic Crystals in a Microgravity Environment," J. Crystal Growth, 76, pp. 673-680, 1986.

2) Radcliffe, M.D., Steffer, J.E., Cook, E.L., Cotting, J.F., Miller, C.R., Drake, M.C., Schroeder, F.S., and Stevens, Jr. D., "Organic Crystals in Low Earth Orbit,"J. Crystal Growth, Vol. 92, pp 581-590, 1988.

3) Duval, W.M.B., Singh, N.B., Glicksman, M.E., "Physical Vapor Transport of Mercurous Chloride Crystals: Design of a Microgravity Experiment," J. Crystal Growth, 174, pp. 120-129, 1997.

4) Raffel, M., Willert, C., Kompenhans, J., Particle Imaging Velocimetry: A Practical Guide, Springer-Verlag, 1998.

5) Cha, S.S., Ramachandran, N., "3-D Flow Field Diagnostics and Validation Studies Using Stereoscopic Tracking Velocimetry," 40th Aerospace Sciences Meeting & Exhibit, AIAA-2002-0454 Paper, Jan. 11-18, 2002.

6) Mullin, J.A., Dahm, W.J.A., "Highly-Resolved Three-Dimensional Velocity Measurements via Dual-Plane Stereo Particle Image Velocimetry (DSPIV) in Turbulent Flows," 40th Aerospace Sciences Meeting & Exhibit, AIAA-2002-0290 Paper, Jan. 11-18, 2002.

7) Kuang, J., Maxworthy, T., "Measurements of Velocity and Streamline Fields of Miscible Displacement in Round Tubes," 40th Aerospace Sciences Meeting & Exhibit, AIAA-2002-0887 Paper, Jan. 11-18, 2002.

8) Bethea, M.D., Lock, J. A., Merat, F., Crouse, P., " Three-dimensional Camera Calibration Technique for Stereo Imaging Velocimetry Experiments", Opt. Eng., 36(12), pp 3445-3454, 1997.

9) Wernet, M. P., Bright, M. M., Skoch, G. J., " An investigation of Surge in a High Speed Centrifugal Compressor Using Digital PIV", Trans. ASME Journal of Turbomachinery, Vol. 123, pp. 418-428, 2001.

10) Lide, D.R., Frederikse, H.P.R., CRC Handbook of Chemistry and Physics, 77th Ed., CRC Press Inc., pp 6-9, 6-10, 1996-1997.

11) Duval, W.M.B., "Numerical Study of Mixing of Two Fluids Under Low Gravity," NASA TM 105865, 1992.

12) Duval, W.M.B., "Flow Field Topology of Buoyancy Induced Mixing,"34th Aerospace Sciences Meeting & Exhibit, AIAA-96-0253 Paper, 1996.